BUILDUP STUDIES OF A TANDEM MIRROR
REACTOR WITH INBOARD THERMAL BARRIERS

G. E. Gryczkowski
J. M. Gilmore

October 9, 1980

Lawrence
Livermore
Laboratory

BUILDUP STUDIES OF A TANDEM MIRROR
REACTOR WITH INBOARD THERMAL BARRIERS*

G. E. Gryczkowski and J. M. Gilmore
Lawrence Livermore National Laboratory
Livermore, California 94550

The build-up and quasi-steady state phases of the operation of the tandem mirror experiment, TMX, and of a tandem mirror machine with inboard thermal barriers, MFTF-B, have been simulated using a fluid model of the central cell and plug plasmas. The fluid model incorporates classical radial transport, three-dimensional cold gas transport in cylindrical geometry, and neutral beam transport corrected for finite-Larmor-orbit effects in both the central cell and yin-yang end plugs.

The results obtained for the TMX simulations agree favorably with experimental data, and the thermal barrier mirror machine simulations indicate that plasma build-up to the densities and temperatures required for such near term experiments, such as MFTF-B, is possible using current neutral beam and ECRH technology.

Introduction

A fluid model of the central cell and plug plasmas, generated by taking velocity moments of the drift-kinetic equation,[1] has been used to perform numerical simulations of the buildup and quasi-steady state phases of the operation of the tandem mirror experiment, TMX,[2] and of a tandem mirror machine with inboard thermal barriers.[3] The thermal barrier tandem mirror machine is shown schematically in Fig. 1. The TMX and thermal barrier mirror machine parameters used are given in Table 1. The fluid model incorporates classical radial transport, three-dimensional cold gas transport in cylindrical geometry, and neutral beam transport corrected for finite-Larmor-orbit effects upon the neutral beam deposition profile in both the central cell and yin-yang end plugs.

The results obtained for the TMX simulations agree favorably with experimental data, and the thermal barrier mirror machine simulations indicate that plasma build-up to the densities and temperatures required for such near term experiments, such as MFTF-B,[4] is possible using
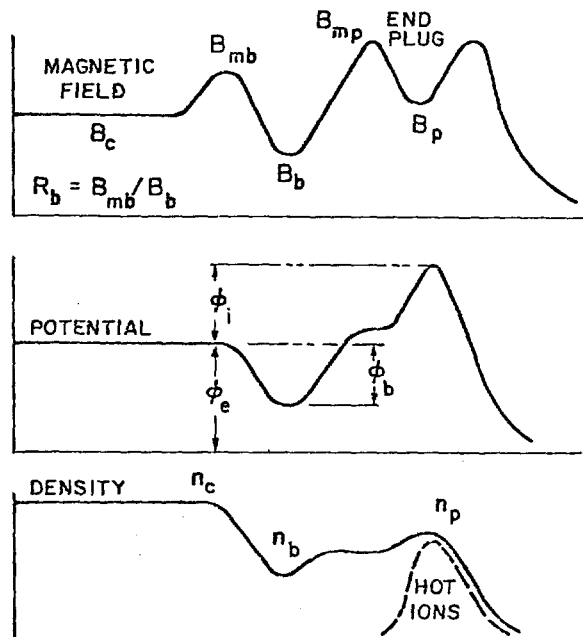
Fig. 1. The magnetic field, potential, and density axial profiles are shown for a tandem mirror machine with inside thermal barriers.

neutral beam injector modules and ECRH guns currently under development. Furthermore, the cold gas attenuation which occurs in the thermal barrier mirror machine simulations indicates that a sufficiently large plasma halo will exist to shield the A-cell region of MFTF-B from excessive electron sources, which would otherwise degrade central cell ion confinement and reduce the effective Q of the machine.

Fluid Model of the Central Cell and Plug Plasmas

By taking velocity moments of the drift-kinetic equation, a set of particle and energy balance equations for the central cell and plug plasmas can be derived. The central cell and plug ion and electron particle balance equations are of the general form:

1

	TMX	Thermal Barrier Mirror Machine
Central Cell Length	314. cm	1500. cm
Plug Length	14. cm	60. cm
Central Cell Magnetic Field Strength	1. KG	15. KG
Barrier Minimum Magnetic Field Strength	-	15. KG
Barrier Mirror Ratio	-	10
Plug Midplane Magnetic Field Strength	10. KG	20. KG
Plug Mirror Ratio	2.	2.
Central Cell Neutral Beam Current	0.A/cm	t < 0.5 sec, 0.22 A/cm @ 50. KeV t > 0.5 sec, 0.018 A/cm @ 60. KeV
Plug Neutral Beam Current	t < 20 ms, 8.21 A/cm @ 11.9 KeV t > 20 ms, 2.5 A/cm @ 19.6 KeV	t < 0.01 sec, 3.34 A/cm @ 50. KeV t < 0.01 sec, 8.34 A/cm @ 15. KeV .01 < t < .5 sec, 3.34 A/cm @ 50. KeV .01 < t < .5 sec, 0.42 A/cm @ 60. KeV t > .5 sec, 0.42 A/cm @ 60. KeV
Central Cell Neutral Gas Current	t < 3ms, 0.13 A/cm t > 3ms, 2.39 A/cm	t < 0.01 sec, 0.2 A/cm .01 < t < 0.5 sec, 1.5 A/cm t > 0.5 sec, 0.5 A/cm
Plug Neutral Gas Current	0.015 A/cm	0.2 A/cm

$$\frac{\partial n}{\partial t} = -\frac{1}{r} \frac{\partial}{\partial r} (r\Gamma) + S - \frac{n^2}{(n\tau)} \qquad (1)$$

where n is the density, Γ is the classical particle flux scaled by an arbitrary multiplicative factor,[5,6] S is the net particle source arising from neutral gas and beam interactions with the plasma, and $n^2/(n\tau)$ is the axial particle loss. The axial loss for electrons and central cell ions is given according to the formulas of Pastukhov and Cohen.[7,8] The plug ion axial loss is given according to the semi-empirical formulas of Logan and Rensink.[9]

The ion and electron energy balance equations are of the general form:

$$\frac{\partial T_j}{\partial t} = \frac{T_j}{rn_j} \frac{\partial}{\partial r} (r\Gamma_j) - \frac{1}{rn_j} \frac{\partial}{\partial r} (rT_j\Gamma_j)$$

$$- \frac{2}{3} \frac{T_j}{r} \frac{\partial}{\partial r} (\frac{r\Gamma_j}{n_j}) - \frac{2}{3} \frac{1}{rn_j} \frac{\partial}{\partial r} (rq_j)$$

$$+ \sum_{\substack{\text{species} \\ i}} \frac{(T_i - T_j)}{\tau^{i/j}} + \left[\frac{dT_j}{dt}\right]_{\substack{\text{END} \\ \text{LOSS}}} - \frac{S_j T_j}{n_j} \qquad (2)$$

where T_j is the temperature of species j, Γ_j is the particle flux, q_j is the heat flux,[5,6] $\tau^{i/j}$ is the classical energy exchange time for rethermalization between species i and species j, $[dT_j/dt]_{\text{END LOSS}}$ is the net axial source or sink of energy for species j, and $S_j T_j/n_j$ is the net source or sink of energy for species j due to neutral beam and gas interactions with the plasma. The axial energy loss for the electrons and central cell ions is computed according to the formulas of Pastukhov and Cohen.[7,8,10] The net plug ion axial energy loss is computed using the Logan-Rensink model.[9]

Equations of the forms given in equations (1) and (2) for central cell ion particle balance, central cell ion energy balance, central cell electron energy balance, plug ion particle balance, plug ion energy balance, and plug electron energy balance are finite differenced in a flux conservative manner and time integrated using a method similar to that used previously by Noulberg[11] in the WHIST tokamak transport code.

In addition to solving for the densities and temperatures, the potentials ϕ_c, ϕ_b, and ϕ_e, indicated in Fig. 1, must also be computed at each time step. ϕ_c, the difference in potential between the central cell and plug mid-

2

planes is computed by equating the rate of de-trapping of plug electrons to the rate of trapping of passing central cell electrons into the plug potential well.[10] ϕ_b, the absolute value of the barrier potential which thermally insulates the plug and central cell electrons, is calculated by requiring charge quasi-neutrality in the barrier region.[12] Finally, ϕ_e, the potential at which the central cell floats relative to ground, is calculated by equating electron loss (both radial and axial) to ion loss (both radial and axial) over the entire machine.

Neutral Gas and Neutral Beam Transport

The three-dimensional transport of neutral gas and neutral beams is simulated by a numerical code which calculates the radial deposition of an external source of molecular neutrals and of the resultant Franck-Condon and charge-exchange neutrals in a cylindrical plasma and which also calculates the radial deposition of an arbitrary array of neutral beams and of the resultant charge-exchange neutrals assuming that the molecular, Franck-Condon, and charge-exchange neutrals are generated with three-dimensional isotropy.

Twelve basic reactions are included in the neutral transport calculations. The molecular neutral/plasma interactions include electron dissociation, electron ionization, ion charge exchange, and ion ionization of the molecular neutrals. The molecular ion/plasma interactions include electron dissociative excitation, electron dissociative ionization, electron dissociative recombination, ion dissociative excitation, and ion dissociative ionization of the molecular ions. The monatomic neutral/plasma interactions, which encompass Franck-Condon neutral, charge-exchange neutral, and neutral beam interactions with the plasma, include electron ionization, ion charge exchange, and ion ionization of the monatomic neutrals.

To determine the neutral transport and deposition for an arbitrary array of neutral beams of arbitrary position, width, and energy, each neutral beam is divided into a set of parallel flight paths determined by the beam width, beam position, and radial mesh spacings. The source strength of each flight path is determined by the total beam source strength and the beam profile (i.e., flat or Gaussian). The trajectory of each flight path is then tracked through the plasma and deposition along the flight path is determined by the local plasma densities and temperatures with appropriate corrections for finite-Larmor-orbit effects.[13,14] The neutral beam current which passes through the plasma without interacting with the plasma is assumed to impact the wall and to be trapped therein.

To determine the neutral transport and deposition for the molecular, Franck-Condon, and charge-exchange neutral sources, it is first necessary to redefine the radial mesh, such that

the mean free paths for the neutrals are greater than or equal to a radial mesh spacing. At the completion of the neutral calculations, the radial mesh is transformed back to its original configuration. It is then assumed that the molecular neutrals enter isotropically at the edge of the plasma. Flight paths for the molecular neutrals are then constructed in three-dimensional space, and the transport and deposition of the neutrals along each flight path are then calculated. The deposition of the molecular neutrals generates Franck-Condon and charge-exchange neutrals, while the neutral beam/plasma interactions are an additional source of charge-exchange neutrals. Source points for the generation of these monatomic neutrals are situated radially throughout the plasma, and neutral flight paths are constructed for each source point in three-dimensional space. The transport and deposition of these neutrals along each flight path are then calculated. Subsequent generations of charge-exchange neutrals are similarly treated. Neutrals which escape from the plasma are assumed to impinge on the wall and to be trapped there.

Computational Results

To verify the physics and numerics of this work, simulation runs using TMX input parameters (Table I) were compared with TMX experimental data (Table II). The simulation run assumes ten times classical diffusion and also no wall reflection of incident neutrals. An examination of Table II shows that the simulation run agrees favorably with the experimental data at equilibrium. The centerline temperatures and potentials are well within the measured ranges, while the densities agree to within a factor of two. Experimental uncertainties as to neutral beam width and gas input as well as numerical deficiencies such as lack of wall reflection and neoclassical diffusion could easily account for the discrepancies.

The time dependence of the central cell ion density on axis is shown in Fig. 2. Note that the density builds up slowly up to ~3 msec within which time the neutral gas current is due to background gas but rises substantially thereafter when the neutral gas current is determined by that from the puffer valves. An equilibrium value is reached at ~10 msec and is sustained until the plug neutral beams are turned off at ~20 msec. The central cell ion density then decays away as the confining potential is degraded. This is very similar to the time-dependent TMX operation.

The central cell ion density, ion temperature and electron temperature radial profiles at t = 20 msec are shown in Figs. 3-5. The inverted density profile in Fig. 3 is not seen in TMX operation. This implies that the 10 x classical diffusion model is insufficient to simulate actual neoclassical diffusion. Note that finite-Larmor-orbit effects and radial transport support the plasma against edge erosion allowing radial

TABLE II: Comparison of TMX Experiment and Simulation

	Experiment (Shot 66)	Simulation
Centerline Center Cell Density	$2.9 \times 10^{12}/cm^3$	$4.32 \times 10^{12}/cm^3$
Centerline Central Cell Ion Temperature	-	35.64 eV
Centerline Central Cell Electron Temperature	-	107.04 eV
Centerline Plug Density	$1.2-1.9 \times 10^{13}/cm^3$	$1.08 \times 10^{13}/cm^3$
Centerline Plug Ion Temperature	8.4 KeV	8.38 KeV
Centerline Plug Electron Temperature	117-335 eV	121.05 eV
Centerline Value of ϕ_e	-	445.43 eV
Centerline Value of ϕ_c	-	93.65 eV
Centerline Value of $\phi_p = \phi_c + \phi_e$	400-550 eV	539.08 eV
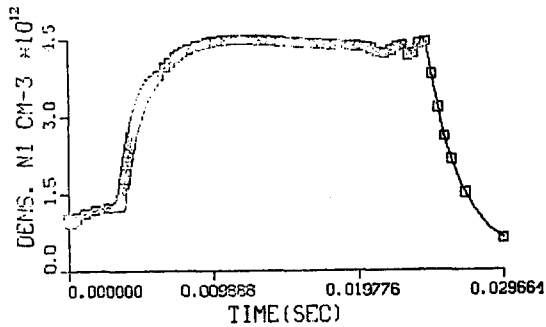
Fig. 2. Time dependence of central cell density on axis for a TMX simulation.
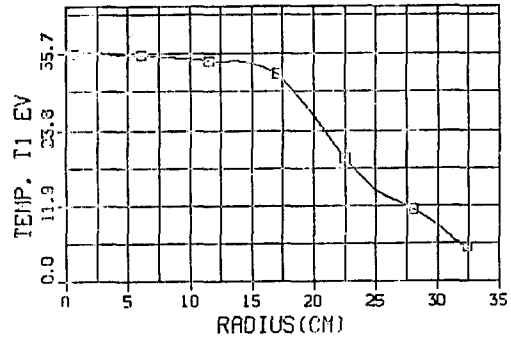
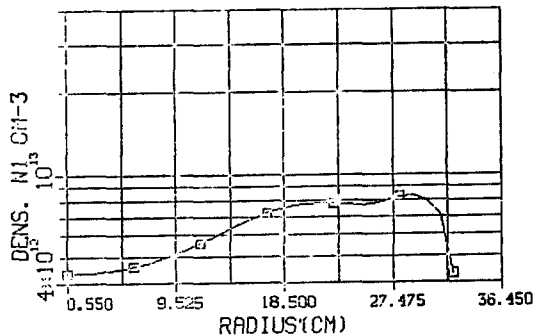Fig. 4. Central cell ion temperature radial profile at t = 0.020 sec for a TMX simulation.

Fig. 3. Central cell ion density radial profile at t = 0.020 sec for a TMX simulation.
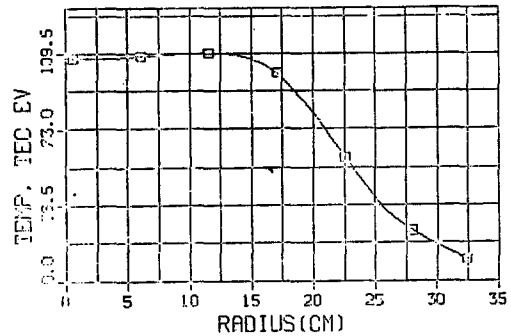

Fig. 5. Central cell electron temperature radial profile at t = 0.020 sec for a TMX simulation.

4

growth to the limiters. The temperature profiles are consistent with TMX measurements. Neutral gas cooling of the plasma perimeter accounts for the rapid decline in ion and electron temperatures from the plasma core.

To model the build-up phase for a tandem mirror machine with inboard thermal barriers, cases were run to simulate the fueling and heating of reactors with MFTF-B parameters (Tables I and III). Table III shows the results of two such runs. Case MFTF5 assumes that the plug ECRH conforms to a Gaussian profile, while case MFTF6 assumes an inverted Gaussian ECRH profile. The radial transport in both the central cell and plugs is assumed to be 10 x classical, and the plug ECRH rise time is assumed to be 0.5 sec in both cases. Ramped ECRH is desirable in order to avoid initially overheating the low density plug plasma. If the plug electrons overheat, the ambipolar hole energy in the plug can become equal to or greater than the neutral beam injection energy, leading to very lossy plug and central cell plasmas. Since ECRH absorption is proportional to $1-\exp(-aT_{ep})$, the system may naturally ramp itself.

Since the electron temperatures on axis of each case are approximately equal at t = 0.5 sec, the initial electron heating is via hot ion drag. At t = 1.0 sec the electron temperatures on axis are much lower for the inverted Gaussian ECRH profile; thus, once the startup neutral beams are turned off and only the sustaining neutral beams are functioning, electron heating is determined by the ECRH deposition in the plug, which is much lower on axis for the inverted Gaussian ECRH profile. The central cell ion temperature on axis drops from t = 0.5 sec to t = 1.0 sec in both cases due to decreased neutral beam heating in the central cell and to the loss of high energy ions out of the central cell. The plug ion temperature on axis rises in both cases due to the preferential loss of low energy ions scattered into the loss cone.

The time dependence of the central cell ion density on axis for $0.0 < t < 0.5$ sec is shown in Fig. 6 for the Gaussian ECRH profile. Note that for $0.0 < t < 0.01$ sec the 10 msec startup neutral beams are operational and direct 11.68 A/cm of neutral beam current on each plug. This neutral beam current causes the confining

TABLE III: MFTF Simulation Cases

	MFTF5	MFTF6
Plug ECRH Power	0.6 MW-Gaussian	0.6 MW-Inverted Gaussian
Plug ECRH Rise Time	0.5 sec	0.5 sec
Transport	10x-classical	10x-classical
Central Cell Ion Density on Axis		
t = 0.5 sec	$1.1 \times 10^{13}/cm^3$	$9.76 \times 10^{12}/cm^3$
t = 1.0 sec	$1.0 \times 10^{13}/cm^3$	$6.5 \times 10^{12}/cm^3$
Central Cell Ion Temperature on Axis		
t = 0.5 sec	9.7 KeV	12.2 KeV
t = 1.0 sec	4.9 KeV	6.7 KeV
Central Cell Electron Temperature on Axis		
t = 0.5 sec	3.6 KeV	3.6 KeV
t = 1.0 sec	11.7 KeV	8.2 KeV
Plug Ion Density on Axis t = 0.5 sec	$7.0 \times 10^{13}/cm^3$	$6.9 \times 10^{13}/cm^3$
t = 1.0 sec	$5.8 \times 10^{13}/cm^3$	$1.56 \times 10^{13}/cm^3$
Plug Ion Temperature on Axis		
t = 0.5 sec	41. KeV	41. KeV
t = 1.0 sec	62. KeV	51.8 KeV
Plug Electron Temperature on Axis		
t = 0.5 sec	4.2 KeV	4.2 KeV
t = 1.0 sec	50. KeV	13.3 KeV

potential, ϕ_c, to increase rapidly, and thus
there is also a rapid increase in central cell
density in the first 10 msec of operation. For
$0.01 < t < 0.5$ sec the neutral beam current in
the plug drops to 3.76 A/cm, and this causes a
much slower rise in central cell density till
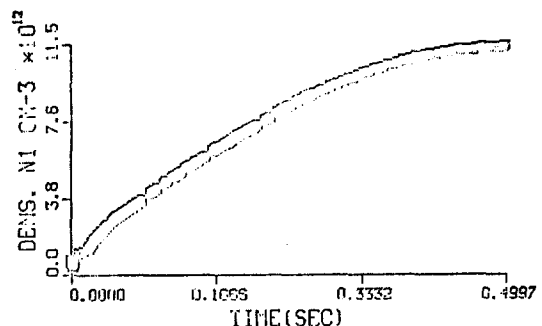equilibrium is attained at ~ 0.5 sec.

Fig. 6.   Time dependence of central cell density
on axis for $0.0 < t < 0.5$ sec for case
MFTF5.

The central cell ion density, ion tempera-
ture, and electron temperature radial profiles
at $t = 0.5$ sec are shown in Figs. 7-9 for the
Gaussian ECRH profile. Note that the ion density
profile shows a slight halo at large radii. A
plasma halo at the plasma perimeter is desirable
to shield the thermal barrier region from ex-
cessive neutral gas penetration. The plasma halo
is supported against neutral erosion by finite-
Larmor-orbit effects on neutral deposition and by
radial plasma transport. The ion and electron
temperatures decrease with increasing radius as
expected due to neutral gas cooling and radial
energy transport.
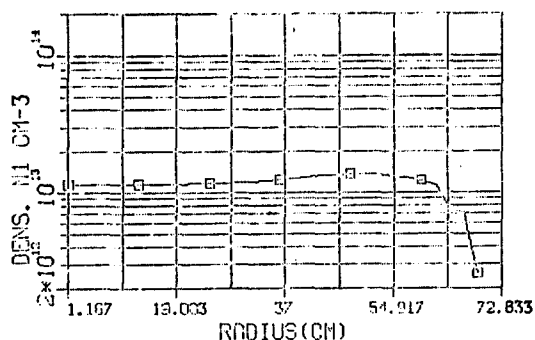
Fig. 7.   Central cell ion density radial profile
at $t = 0.5$ sec for case MFTF5.
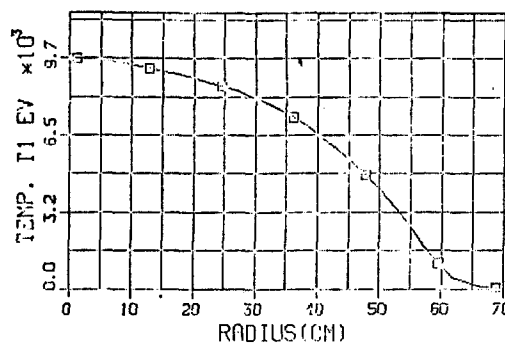
Fig. 8.   Central cell ion temperature radial
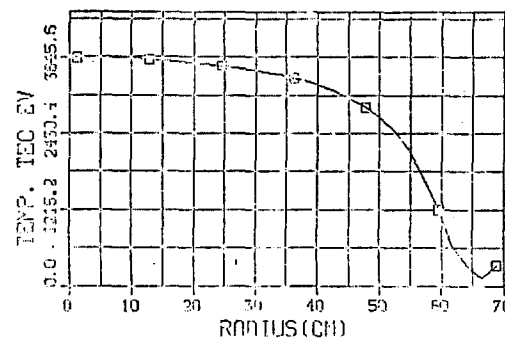profile at $t = 0.5$ sec for case MFTF5.

Fig. 9.   Central cell electron temperature
radial profile at $t = 0.5$ sec for case
MFTF5.

The time dependent behavior of the central
cell ion density on axis for $0.5 < t < 1.0$ sec is
shown in Fig. 10 for the Gaussian ECRH profile.
Since the startup neutral beams in the central
cell and plugs are turned off at $t = 0.5$ sec
leaving only the 0.42 A/cm and 0.018 A/cm sus-
taining neutral beams in the plugs and central
cell, respectively, and since the plug neutral
gas current is decreased to 0.5 A/cm after 0.5
sec of operation, the plasma density initially
declines; however, it quickly establishes a new
but lower equilibrium value as the plasma read-
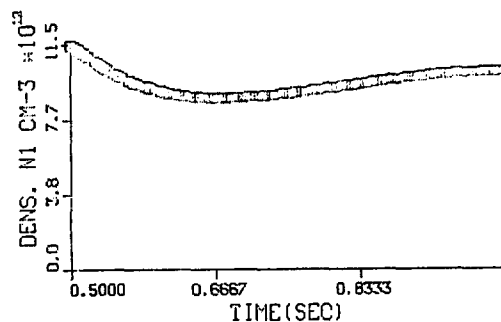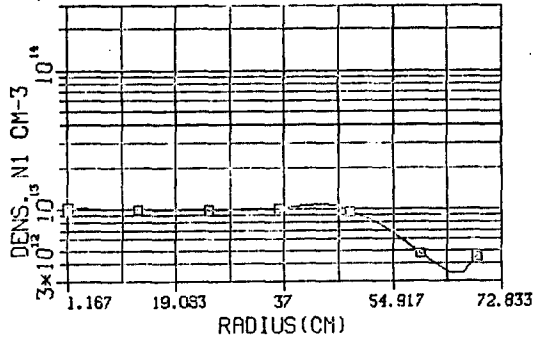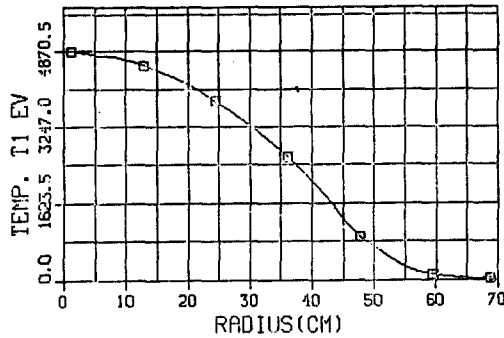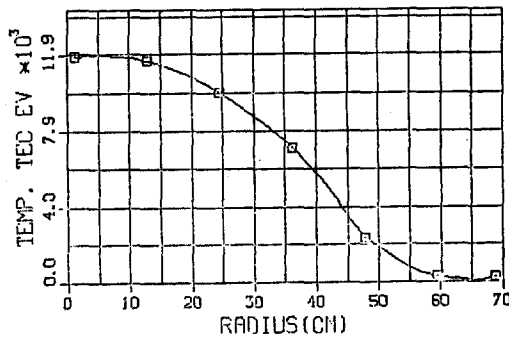justs to the new operating conditions.

Fig. 10. Time dependence of central cell density
on axis for $0.5 < t < 1.0$ sec for case
MFTF5.

The central cell ion density, ion tempera-
ture, and electron temperature radial profiles at
t = 1.0 sec are shown in Figs. 11-13 for the
Gaussian ECRH profile. Note that the ion density
profile remains relatively unchanged from that at
t = 0.5 sec. The ion and electron temperature
profiles, however, have much steeper gradients
with increasing radius. This results from the
fact that the Gaussian ECRH deposition in the
plugs must support the electron temperatures due
to less neutral beam deposition in the central
cell and plugs.

To determine the effects of the ECRH deposi-
tion profile about which there is some uncer-
tainty, an inverted Gaussian ECRH deposition pro-
file was modeled (Case MFTF6). The time depen-
dence of the central cell ion density on axis for
$0.5 < t < 1.0$ sec is shown in Figs. 14 & 18 for
the inverted Gaussian ECRH profile and exhibits
similar behavior to that of the Gaussian ECRH
profile results (Figs. 6 and 10). This implies
that for the first 0.5 sec of operation the
plasma build-up and heating is dominated by the
startup neutral beams in the central cell and
plugs and that for the remaining 0.5 sec of oper-
ation the lower neutral beam and neutral gas
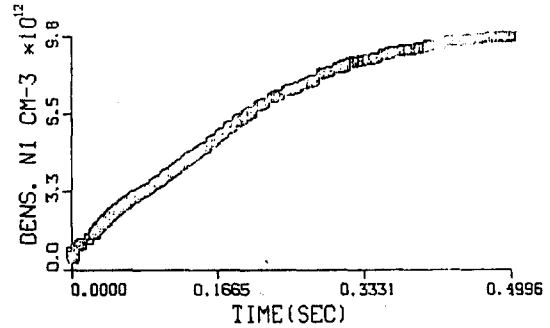currents effect lower centerline density values.

Fig. 11. Central cell ion density radial profile
at t = 1.0 sec for case MFTF5.

Fig. 12. Central cell ion temperature radial
profile at t = 1.0 sec for case MFTF5.

Fig. 13. Central cell electron temperature
radial profile at t = 1.0 sec for case
MFTF5.

Fig. 14. Time dependence of central cell density
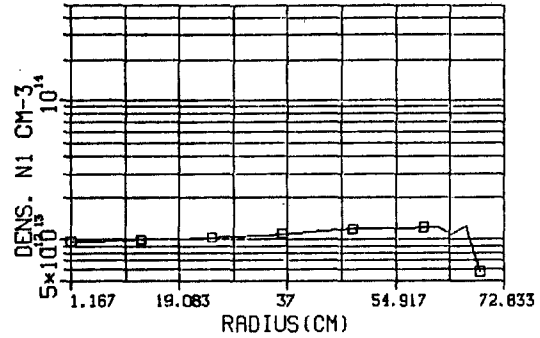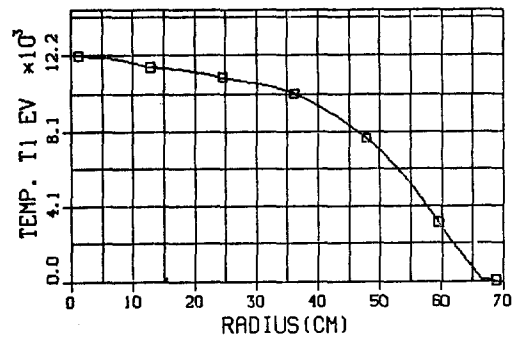on axis for $0.0 < t < 0.5$ sec for case
MFTF6.

Fig. 15. Central cell ion density radial profile
at t = 0.5 sec for case MFTF6.

Fig. 16. Central cell ion temperature radial
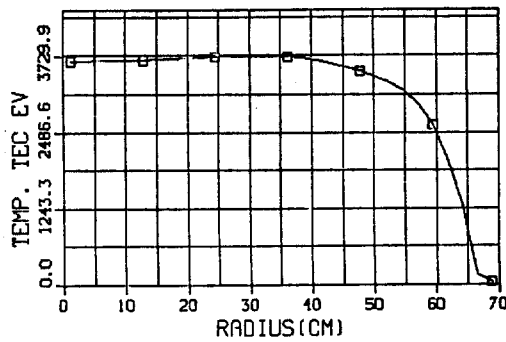profile at t = 0.5 sec for case MFTF6.

Fig. 17. Central cell electron temperature
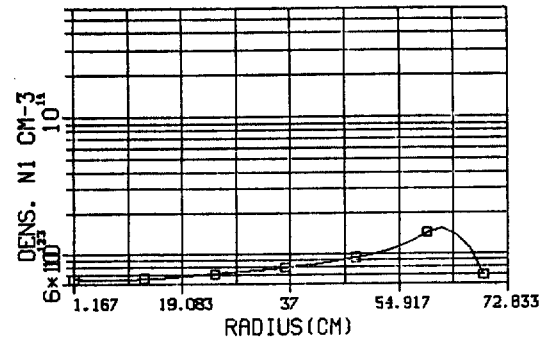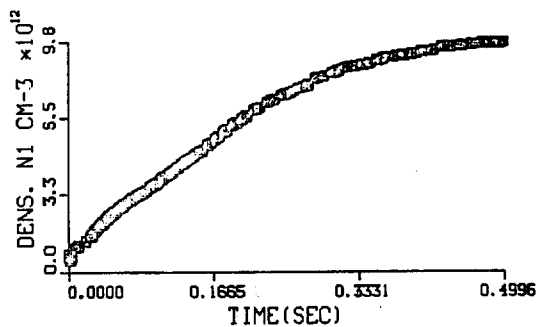radial profile at t = 0.5 sec for case
MFTF6.

Fig. 18. Time dependence of central cell density
on axis for $0.5 < t < 1.0$ sec for MFTF6.

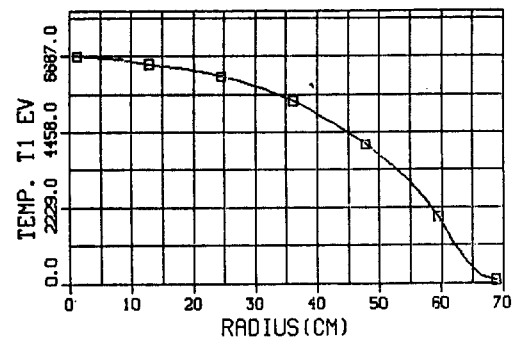Fig. 19. Central cell ion density radial profile
at t = 1.0 sec for case MFTF6.

Fig. 20. Central cell ion temperature radial
profile at t = 1.0 sec for case MFTF6.

Fig. 21. Central cell electron temperature
radial profile at t = 1.0 sec for case
MFTF6.

The central cell ion density, ion temperature
and electron temperature radial profiles at t =
0.5 sec and t = 1.0 sec are shown in Figs. 15-17
and 19-21 for the inverted Gaussian ECRH deposi-
tion profiles. The ion density profile is
slightly inverted at t = 0.5 sec and shows
similar behavior to the Gaussian ECRH deposition
profile results (Fig. 11); however, at t = 1.0
sec the ion density profile is deeply inverted.
The electron temperature profile is also slightly
inverted at t = 0.5 sec but deeply inverted at t
= 1.0 sec. Thus, the ECRH deposition profile has
minimal effect on plasma characteristics when
large neutral beam currents impinge on the plasma
but much larger effects when the large beam
currents are absent (i.e., during steady state
operation). The ion temperature profiles display
no inverted structure at either t = 0.5 sec or
t = 1.0 sec. Thus neutral beam heating of the
plasma ions dominates drag off of the hot
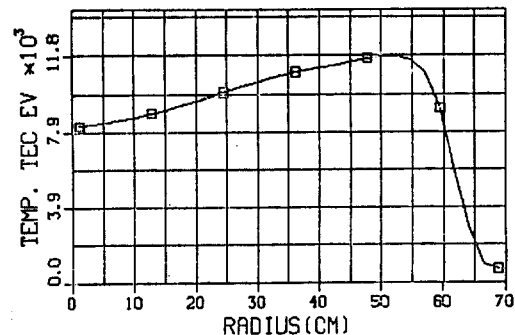electrons at all times, even for low neutral
beam currents.

Conclusions

The following conclusions resulted from the
aforementioned TMX and MFTF-B simulation runs:

1. A comparison of TMX simulation runs with TMX experimental results shows that the physics and numerics of the present work model the behavior of tandem mirror machines to within experimental tolerances.
2. Although a plasma halo is seen in both TMX and MFTF simulation runs, the addition of neoclassical transport and a realistic wall reflection model could modify this result substantially.
3. Finite-Larmor-orbit effects and radial plasma transport support the plasma edge against erosion and allow radial growth to the limiters in both TMX and MFTF-B simulation runs.
4. Initial build-up of the central cell and plug plasmas is determined by the neutral beam injection currents, energies, and aiming patterns.
5. In MFTF-B simulation runs with ramped ECRH, the initial electron heating is via hot ion drag. After the start-up beams are turned off and only the sustaining beams are in use, electron heating is determined by the ECRH deposition in the plugs. Inverted ECRH deposition profiles produce inverted temperature and potential profiles which may be desirable if large plasma halos are a requirement for MFTF-B operation.
6. Ramped ECRH is desirable in order to avoid initially overheating the low density plug plasma. If the plug electrons overheat, the ambipolar hole energy in the plug can become equal to or greater than the neutral beam injection energy, leading to very lossy plug and central cell plasmas. Since ECRH absorption is proportional to $[1-\exp(-aT_{ep})]$, the system may naturally ramp itself.
7. Within the limits of the present model, plasma build-up to the densities and temperatures envisaged for the inboard thermal barrier version of MFTF-B is possible.

References

1. P.H. Rutherford, *Physics of Fluids*, 13, 2 (1970).

2. F.H. Coensgen, Lawrence Livermore Laboratory Rept. LLL-Prop.-148 (1977).

3. G.A. Carlson, et al., Lawrence Livermore Laboratory Rept. UCRL-52836 (1979).

4. D.E. Baldwin, ed., Lawrence Livermore Laboratory Rept. UCID-18496 (1980).

5. S.I. Braginskii, "Transport Processes in a Plasma", *Reviews of Plasma Physics*, 1, 205, Consultants Bureau, NY (1965).

6. D.D. Ryutov and G.V. Stupakov, *Fiz. Plazmy*, 4, 3 (1978).

7. V.P. Pastukhov, *Nuclear Fusion*, 14, 3 (1974).

8. R.H. Cohen, M.E. Rensink, T.A. Cutler, and A.A. Mirin, *Nuclear Fusion*, 18, 1229 (1978).

9. B.G. Logan and M.E. Rensink, Lawrence Livermore Laboratory Memorandum MFE/CP/78-181 (1978).

10. R.H. Cohen, I.B. Bernstein, J.J. Dorning, and G. Rowlands, Lawrence Livermore Laboratory Rept. UCRL-84147 (1980).

11. W.A. Noulberg and R.W. Conn, *Nuclear Science and Engineering*, 64, (1977).

12. J. Kesner, University of Wisconsin Rept. UWFDM-303 (1979).

13. A.H. Futch, W. Heckrotte, C.C. Damm, J. Killeen, and L.E. Mish, *Physics of Fluids*, 5, 1277 (1962).

14. B.W. Stallard, Lawrence Livermore Laboratory Rept. UCRL-51784 (1975).